Atomic-scale segregation behavior of Pr at a ZnO [0001] Σ49 tilt grain boundary

Yukio Sato,[1] Teruyasu Mizoguchi,[2] Naoya Shibata,[2,3] Takahisa Yamamoto,[1,4] Tsukasa Hirayama,[1] and Yuichi Ikuhara[1,2,5]
[1]*Nanostructures Research Laboratory, Japan Fine Ceramics Center, Atsuta, Nagoya 456-8587, Japan*
[2]*Institute of Engineering Innovation, The University of Tokyo, Bunkyo, Tokyo 113-8656, Japan*
[3]*PRESTO, Japan Science and Technology Agency, Kawaguchi, Saitama, 332–0012, Japan*
[4]*Department of Advanced Materials Science, The University of Tokyo, Kashiwa, Chiba 277-8651, Japan*
[5]*WPI Advanced Institute for Materials Research, Tohoku University, Sendai 980-8577, Japan*
(Received 13 December 2008; revised manuscript received 9 March 2009; published 28 September 2009)

The atomic arrangement and segregation of Pr dopants at a ZnO [0001] Σ49 grain boundary were investigated by *Z*-contrast scanning transmission electron microscopy and first-principles calculations. Scanning transmission electron microscopy revealed that Pr selectively segregated at three kinds of the grain boundary atomic sites. It was found that atomic arrangement of the Pr-doped ZnO [0001] Σ49 grain boundary was similar to that of the undoped GB, and Pr substituted at three kinds of Zn sites at the grain boundary. Comparison of the experimental image with the structure of the undoped grain boundary revealed that the Zn-O interatomic distances are the longest at these Zn sites. There was a tendency for lengths and electronic structures of Pr-O bonds at the Pr-doped ZnO Σ49 grain boundary, when compared with those in the Pr-doped ZnO crystal bulk, to be closer to those in the stable Pr_2O_3 crystal phases.

DOI: 10.1103/PhysRevB.80.094114 PACS number(s): 61.72.Mm, 68.35.Dv, 68.37.Lp

I. INTRODUCTION

Physical properties of ceramics are often influenced by grain-boundary (GB) segregations of dopant atoms. Recent advance in electron microscopy has enabled direct observation of dopant atoms at GBs,[1–5] and segregation effects on the properties have been discussed.[1–4] However, underlying atomic-scale mechanism for GB segregation still remains unclear. It has been suggested that size misfit is a dominant factor for GB segregation in metals.[6] According to this concept, dopant atoms that have much larger atomic size than that in host materials segregate to the atomic sites of longer interatomic distance at the GBs.[6] Although this concept may be also applicable to ceramic materials,[1,4,5] it has been pointed out that electronic effect such as bonding state could be an important factor for GB segregation.[6] However, relationship between GB segregation and the electronic structures has not been well investigated so far.

ZnO ceramics has been used as varistors for electronic devices because of the highly nonlinear current-voltage characteristics.[7] GBs in ZnO varistors play central roles for the electrical properties. In particular, it is considered that the presence of Pr or Bi at the ZnO GBs is a key to obtain better electrical properties.[7] Although we have previously suggested a principal role of Pr on the electrical properties,[4] the dominant factor for the location of segregated Pr was not fully understood. In this study, we investigated atomic arrangement and Pr segregation of the ZnO [0001] Σ49 GB. According to Coincidence Site Lattice theory[8] of GB, Σ values are related to the structural periodicity along the GBs. Since the ZnO Σ49 $(35\bar{8}0)$ GB has a large Σ value and a relatively long structural periodicity along the GB plane,[8] segregation of Pr at several GB atomic sites may be expected. This would be suitable for a systematic investigation on atomic site dependence of GB segregations. Atomic arrangement and Pr segregation of ZnO [0001] Σ49 GB were observed by scanning transmission electron microscopy (STEM). First-principles calculations of undoped and Pr-doped ZnO Σ49 GBs were also performed, and the results were compared with the experimental STEM observations.

II. METHODOLOGY

A. Experimental procedures

A ZnO bicrystal with a Pr-doped [0001] Σ49 symmetric tilt GB was fabricated. Rotation angle around [0001] was $\sim 16.6° \pm 0.1°$ (measured from the selected area diffraction pattern taken from the GB region of the ZnO bicrystal), and the GB planes were $\{35\bar{8}0\}$ of both crystals. The fabrication procedure was described elsewhere,[4] although orientation relationship and GB plane in the present study were different from those of Ref. 4. Thin foils for STEM observations were obtained from the ZnO bicrystal by conventional procedure including mechanical polishing, dimple grinding, and Ar-ion beam milling. The bicrystal specimens were mechanically polished down to ~ 30 μm, and then, center parts of the specimens were dimpled down to ~ 20 μm. The specimens were thinned by Ar-ion beam milling using PIPS (Model 691, Gatan Inc.) with the acceleration voltages of $3 \sim 4$ kV to obtain electron transparency. They were finally milled by low-voltage Ar-ion beam milling with the acceleration voltage of 1 kV using the Model 1010 (Fischione Instruments, Inc.). STEM observations were performed using JEM-2100F (JEOL Ltd.) with a spherical aberration corrector (CEOS Gmbh). For high-angle annular dark-field (HAADF) STEM observations, convergence semiangle of the electron probe was ~ 22 mrad., and detection angle for HAADF detector was higher than 80 mrad. Electron energy loss spectra (EELS) were acquired by Enfina spectrometer (Gatan Inc.) in EM-002BF transmission electron microscope (Topcon Co.). EELS were taken from the area including the Pr-doped GB. Size of electron probes used for the EELS measurement was ~ 1 nm.

 ©2009 The American Physical Society

TABLE I. Comparison between the calculated and the experimental structural parameters for ZnO, and *A*-type Pr_2O_3 and *C*-type Pr_2O_3 crystals bulk. Lattice constants and internal parameters are shown. Space group for ZnO, *A*-type Pr_2O_3, and *C*-type Pr_2O_3 are $P6_3mc$, $P\bar{3}m1$, and $Ia3$, respectively.

	a (Å)	c (Å)			z_O
ZnO (In this study)	3.294		5.303		0.380
ZnO (Calculation)[a]	3.287		5.279		0.381
ZnO (Calculation)[b]	3.286		5.299		
ZnO (Experiment)[c]	3.242		5.188		0.382
	a (Å)	c (Å)		z_{Pr}	z_O
A-Pr_2O_3 (In this study)	3.904	6.138		0.249	0.645
A-Pr_2O_3 (Calculation)[d]	3.895	6.126		0.248	0.645
A-Pr_2O_3 (Experiment)[e]	3.859	6.013		0.246	0.656
	a (Å)	x_{Pr}	x_O	y_O	z_O
C-Pr_2O_3 (In this study)	11.299	0.969	0.390	0.149	0.378
C-Pr_2O_3 (Calculation)[d]	11.288	0.967	0.391	0.149	0.379
C-Pr_2O_3 (Experiment)[f]	11.152	0.965	0.385	0.145	0.380

[a]Reference 12.
[b]Reference 13 (calculated by the GGA-PBE potential).
[c]Reference 14 (measured at 20 K).
[d]Reference 15.
[e]Reference 16.
[f]Reference 17.

B. Theoretical procedures

First-principles band-structure calculations were performed using the plane-wave basis projector-augmented wave method[9] in the VASP code.[10] The calculations were performed under three-dimensional periodic boundary conditions. Generalized gradient approximation (GGA)[11] was used for the exchange-correlation potentials. Stable atomic structures of *A*-type and *C*-type Pr_2O_3 crystals, Pr-doped ZnO crystal bulk, and undoped and Pr-doped ZnO [0001] $\Sigma 49$ GBs were calculated. It has been reported that there are two kinds of stable crystal structures for Pr_2O_3 in the temperature range used for the present experiments.[12] One of the structures is a hexagonal crystal structure, which is called "*A*-type" Pr_2O_3. The other one is a cubic structure, which is called "*C*-type" Pr_2O_3. Besides, according to the reported phase diagram,[13] ZnO-Pr_2O_3 system showed eutectic type phase diagram, and there were no other compounds composed of Zn, Pr, and O. Thus, *A*-type and *C*-type Pr_2O_3 were chosen for stable Pr_2O_3 crystal phases in this study. Unit cells of ZnO crystal bulk and *A*-type and *C*-type Pr_2O_3 crystals bulk containing 4, 5, and 40 atoms, respectively, were calculated. Table I shows calculated lattice constants for ZnO and Pr_2O_3 crystals in this study. The obtained values are compared with previous reports by experiments and first-principles calculations with GGA approximation. Obtained values in this study were consistent with the previous reports.[14–19] For Pr-doped ZnO bulk, ZnO supercell containing 192 atoms was constructed by replicating the ZnO bulk unit cell by $4\times4\times3$, and a Zn was replaced with a Pr. Concentration of Pr in the supercell is roughly about 1 cation % in this case.

Stable atomic arrangement for the undoped ZnO $\Sigma 49$ GB was optimized using the VASP code. For these calculations, stable atomic arrangement of the undoped ZnO $\Sigma 49$ GB was firstly obtained by the static lattice calculation with the GULP code[20] using the 224-atom supercell. Procedure of the calculations was described elsewhere.[21] After that, the obtained atomic arrangement was used as an initial input for the VASP calculations. Figure 1 shows a supercell for the undoped ZnO $\Sigma 49$ GB used in the present study. Two equivalent GBs were included in the supercell. They are at the middle and the edge of the supercell. Considering the structural periodicity along x and z directions, lengths of the supercell along x and z directions were fixed to be 23.0553 Å(x) and 5.3033 Å(z). On the other hand, calculations with some different lengths along y direction were performed to consider the effect of GB expansion. As a result, length along y direction was optimized to be 22.5983 Å(y). Supercells with y lengths of $22.5983+0.2$ Å(y) and $22.5983-0.2$ Å(y) showed 0.30 and 0.67 eV higher energies, respectively.

Then, stable atomic arrangement for Pr-doped ZnO $\Sigma 49$ GB was calculated using the VASP code. For these calculations, the obtained supercell for the undoped ZnO $\Sigma 49$ GB was doubled in z direction to reduce the interactions among Pr in adjacent supercells. Thus, the supercell contained 448 atoms, and its size became 23.0553 Å(x) $\times$ 22.5983 Å(y) $\times$ 10.6066 Å(z). Structural optimization was performed after replacing Zn with Pr. Atomic position in the supercell was relaxed, while volume of the supercell was fixed. Replacing

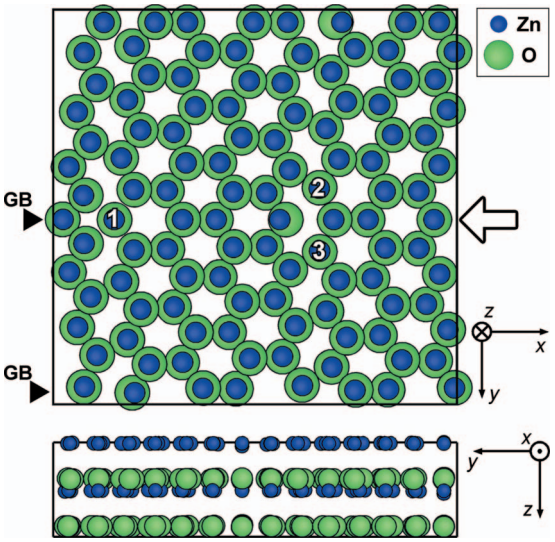

FIG. 1. (Color) Atomic arrangement of undoped ZnO Σ49 GB obtained by first-principles calculations. Rectangles indicate dimensions of the supercells. Blue and green circles show Zn and O. Lattice vectors of the supercells are also shown. ⟨0001⟩ of both ZnO crystals correspond to z direction in the figures. Two equivalent GBs in the supercell are shown by black arrows. Upper panel shows the structure viewed along z direction, and the same structure is viewed from the white bold arrow's direction in the lower panel.

of Zn with Pr was performed for one GB at the middle of the supercell but was not performed for the other GB at the edge of the supercell. During the optimizations for Pr-doped GB, change of atomic positions for the other GB in the supercell was only about 0.03 Å. Thus, we assumed that change of atomic structures and energies for the other GB are negligible. According to the experimental HAADF STEM images, three atomic columns (1, 2, and 3 in Fig. 1), were considered for segregation of Pr. In this GB supercell, two Zn and two O are aligned in an atomic column when it is projected along z direction. One of two Zn in the atomic column 1 was replaced with a Pr, and the same things were done for the atomic columns 2 and 3. Configurations of the three Pr in the supercell were also considered, which is discussed later. It was assumed that formal valency of Pr was 3+, which is consistent with the EELS results taken from the Pr-doped ZnO Σ49 GB as will be described later. Structural optimization was performed until residual forces had converged to less than 0.02 eV/Å. Cutoff energy for plane-wave basis sets was 400 eV for all the cases. Brillouin-zone integrations were performed by $1\times1\times4$ (undoped ZnO Σ49 GB), $1\times1\times2$ (Pr-doped ZnO Σ49 GBs), $3\times3\times3$ (C-type Pr_2O_3 and Pr-doped ZnO crystals bulk), $10\times10\times6$ (ZnO crystal bulk), and $7\times7\times4$ (A-type Pr_2O_3 crystal bulk) k-point mesh generated by Monkhorst-Pack scheme.[22]

III. RESULTS AND DISCUSSION

Firstly, we performed low-magnification STEM observation of the ZnO bicrystal. It was found that two ZnO crystals are well bonded at most of the GB region, although the precipitates of praseodymium oxide were partly present. Such

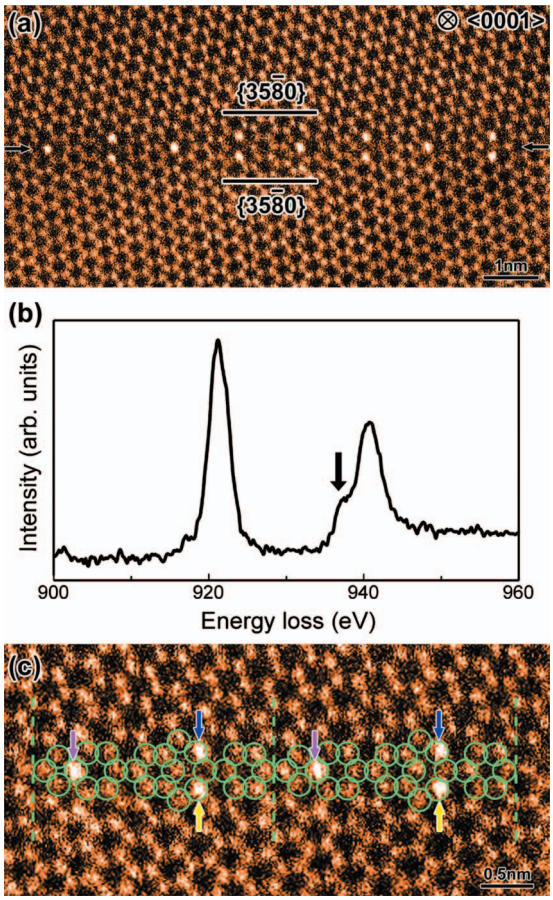

FIG. 2. (Color) (a) HAADF STEM image of the Pr-doped ZnO Σ49 GB. Incident beam direction and GB plane are parallel to ⟨0001⟩ and $\{35\bar{8}0\}$ of both crystals, respectively. Arrows show the position of GB plane. (b) Pr-$M_{4,5}$ edge EELS taken from a region including the GB. Two main peaks in the spectrum show Pr-M_5 and M_4 edges. A shoulder appeared at the left side of the M_4 edge, which is indicated by the arrow. (c) Enlarged HAADF STEM image with the framework structure of undoped ZnO Σ49 GB, which is superimposed by green circles. Dotted lines show the periodicity along the GB plane. Colored arrows indicate the location of much brighter spots. Three different colors show three different GB atomic sites.

partly formation of praseodymium oxides were also previously reported for the Pr and Co-doped ZnO GBs.[23] Presence of precipitates indicates that Pr is saturated at the GB. Figure 2(a) shows a typical HAADF STEM image of the Pr-doped ZnO Σ49 GB. Zn and O are aligned in the same atomic columns when they are viewed from ⟨0001⟩ projection. In our experimental conditions, positions of the Zn-O columns appeared as bright spots. This would be because of the incoherent nature of HAADF STEM imaging.[24] Thus, atomic structure of the Pr-doped ZnO Σ49 GB can be directly understood the HAADF STEM image. Besides, much brighter spots are recognized at the Pr-doped ZnO Σ49 GB in the HAADF STEM image. Since intensity of bright spots in HAADF STEM images increases as the atomic number (Z) of atoms included in the columns increases,[25] much brighter spots indicate the presence of heavier atoms than Zn (Z=30), in this case Pr (Z=59). Figure 2(b) shows the

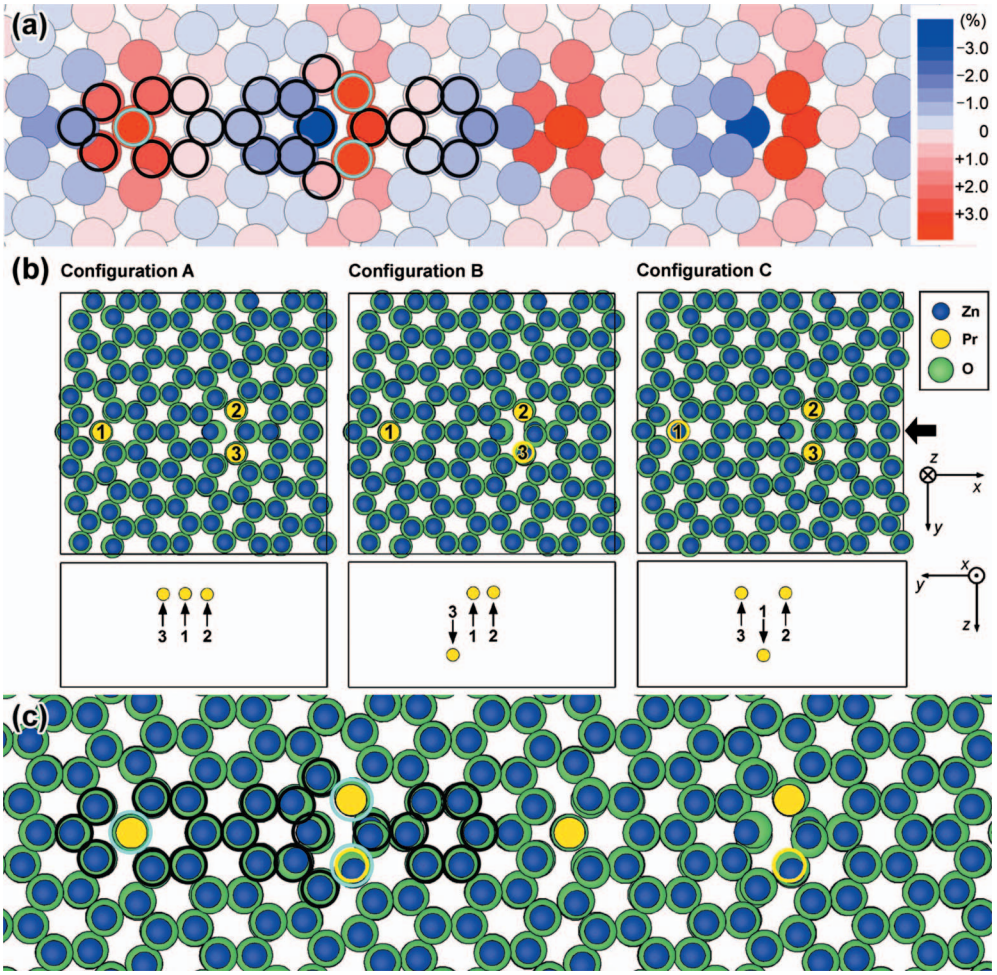

FIG. 3. (Color) (a) Interatomic distance at individual Zn sites of undoped ZnO Σ49 GB. Average interatomic distance with the nearest neighbor O was estimated using the undoped-GB atomic arrangement. Red and blue circles indicate longer and shorter inter-atomic distance than those in ZnO perfect crystal, respectively. (b) Atomic arrangements of Pr-doped ZnO Σ49 GB with three different configurations (*A*-*C*) obtained by first-principles calculations. Rectangles indicate dimensions of the supercells. Upper panels show the structures viewed along the *z* direction, and the lower panels show only Pr's positions viewed from the bold arrow's direction. Three different Pr are shown by three different numbers (1–3). Yellow open circles [Pr(**3**) in *B* and Pr(1) in *C*] indicate the Pr being below Zn and O at the atomic columns. (c) Stable atomic arrangement of Pr-doped ZnO Σ49 GB with the configuration *B*. In (a) and (c), sets of open circles show the framework structure of the GB, and light-blue ones indicate the positions of Pr found in the HAADF STEM images in Fig. 2(c).

Pr-$M_{4,5}$ edge EELS that was taken from a region including the Pr-doped ZnO Σ49 GB. Peaks of Pr-$M_{4,5}$ edges were detected at the GB, again showing the presence of Pr at the GB. In addition to two main peaks showing Pr-M_5 and M_4 edges, there is a shoulder at the left side of the Pr-M_4 edge. Presence of the shoulder indicates that the Pr exists as the 3+ state.[26,27] This result is consistent with our previous study on Pr-doped ZnO Σ7 GB.[4] It is found that Pr segregates at the specific atomic columns of the ZnO Σ49 GB, and there is a unique periodicity for the atomic location of Pr. From the left to the right, Pr locates at one and two atomic columns alternatively along the GB plane. It will be shown that this unique configuration of Pr is closely related to the GB atomic structure. The HAADF STEM image was compared with the theoretically obtained stable atomic structure of undoped ZnO Σ49 GB in Fig. 2(c). Positions of Zn-O columns of the undoped ZnO Σ49 GB match with bright spots of the HAADF STEM image. This suggests that framework structure of the ZnO Σ49 GB did not significantly change with the Pr doping, and Pr substitute at Zn sites in the atomic columns. Considering the periodicity along the ZnO Σ49 GB, Pr segregates at three kinds of atomic columns of the GB as shown by colored arrows in Fig. 2(c). Since this GB is saturated by Pr, it is considered that Pr does not occupy other GB sites in the present experimental conditions.

In order to investigate the relationship between the size misfit and Pr segregation, the map of the Zn-O interatomic distance at individual Zn sites of the undoped ZnO Σ49 GB is shown in Fig. 3(a). It can be seen that three kinds of Zn sites show the longest Zn-O interatomic distance. Position of these Zn sites is consistent with the location of Pr in Fig. 2(c). Thus, it can be regarded that Pr substituted at the Zn sites of the interatomic distances at the ZnO Σ49 GB. This can be roughly explained by the concept of size misfit between Pr and Zn (Ref. 28) as introduced above.

For further understanding, atomic arrangement of Pr-doped ZnO Σ49 GBs was calculated by first-principles calculations. Calculations of Pr-doped ZnO Σ49 GBs were performed after replacing three Zn with three Pr as described in the former section. In this case, there are three possible configurations of Pr, considering the mirror symmetry with respect to the GB plane. Figure 3(b) shows the optimized atomic arrangements for the three different configurations (*A*-*C*). Three Pr are in similar *z* position in the configuration *A*. On the other hand, one Pr is in different *z* position from the others in the configurations *B* and *C*. As the results, two Pr (2 and 3) are close to each other in the configurations *A* and *C*. All three configurations showed similar atomic framework structures. However, total energy calculations revealed that the configuration *B* was the most stable among these three configurations. Hence, Pr-doped ZnO Σ49 GB with the configuration *B* was used as the stable structure in this study. Figure 3(c) shows stable atomic arrangement of the Pr-doped ZnO Σ49 GB that was obtained from the configuration *B*. Since the obtained structure and location of Pr fitted with the experimental HAADF STEM image shown in Fig. 2(c), the obtained structures are used for further analyses as follows.

In order to understand atomic and electronic environment around Pr, we analyzed coordination structure around Pr and valence charge density profile (VCDP) along Pr-O bonds at the Pr-doped ZnO Σ49 GB and in Pr-doped ZnO, *A*-type Pr_2O_3, and *C*-type Pr_2O_3 crystals bulk. It is considered that Pr-doped ZnO crystal bulk has a relatively unstable structure because solid solubility of Pr into ZnO is fairly low.[13] Figures 4(a)–4(d) show coordination structures around Pr in those four models. Pr is four-fold coordinated with O in Pr-doped ZnO crystal bulk, where lengths of the four Pr-O bonds were ~2.26 Å [Fig. 4(a)]. Pr is seven-fold coordinated with O, having three different Pr-O bond lengths of ~2.35 Å, ~2.43 Å, and ~2.72 Å in *A*-type Pr_2O_3 bulk [Fig. 4(b)]. There are two kinds of Pr sites in *C*-type Pr_2O_3 crystal bulk [Fig. 4(c)]. Both are six-fold coordinated with O, but one (left) has identical Pr-O bond length of ~2.43 Å and the other (right) has three Pr-O bond lengths of ~2.40 Å, ~2.41 Å, and ~2.49 Å. At Pr-doped ZnO Σ49 GB (Fig. 4(d)), three different Pr sites, which are named Pr(1), Pr(2), and Pr(3) according to the numbers in Fig. 3(b), are present. All three Pr have five-fold coordination, where the average distance was ~2.36 Å for Pr(1) and ~2.37 Å for Pr(2) and Pr(3). For Pr(2) and Pr(3), one of the Pr-O bonds (dotted lines) is longer than the others.[29] Lengths of Pr-O bonds at the Pr-doped ZnO Σ49 GB, when compared with those in Pr-doped ZnO crystal bulk, tended to be commonly closer to those in *A*-type and *C*-type Pr_2O_3 crystals bulk. There is also a tendency for number of neighboring O around Pr at the ZnO Σ49 GB, when compared with that in Pr-doped ZnO crystal bulk, to be closer to those in *A*-type and *C*-type Pr_2O_3 bulks. As also noted above, numbers of neighboring O around Pr were seven (*A*-type Pr_2O_3), six (*C*-type Pr_2O_3), five (at the ZnO Σ49 GB), and four (in ZnO bulk).

Figures 4(e)–4(g) show VCDPs along the Pr-O bonds in Pr-doped ZnO [Fig. 4(e)], *A*-type Pr_2O_3 [Fig. 4(f)], and *C*-type Pr_2O_3 [Fig. 4(g)] bulks. Four Pr-O bonds in Pr-doped ZnO bulk showed similar VCDPs to one another whereas different profiles appeared in *A*-type and *C*-type Pr_2O_3 crystals bulk. The difference in VCDPs for Pr-doped ZnO bulk would be due to that fact that the Pr-O bond lengths in Pr-doped ZnO bulk are quite different from those in stable Pr_2O_3 crystals bulk. Figures 4(h)–4(j) show VCDPs along the Pr-O bonds at Pr-doped ZnO GB. VCDPs along Pr-O bonds at Pr-doped ZnO GB, when compared with those in Pr-doped ZnO crystal bulk (purple), tend to approach those in stable Pr_2O_3 crystals bulk (blue and green). Thus, it is considered that electronic structure of Pr-O bonds at Pr-doped ZnO GB, when compared with that of Pr-O bonds for Pr in ZnO crystal bulk, tends to be closer to those in stable Pr_2O_3 crystals bulk. These results indicate that Pr selectively substitutes the specific GB Zn sites because these sites can allow Pr atoms to relax its atomic and electronic environment similar to its stable oxides' form. This should be a reason why normally insoluble atoms such as Pr can dissolve and segregate at the GBs in ZnO. It is worth noting that we obtained similar tendency for the Pr at ZnO Σ7 GB.[4] (Detailed structure for the Pr-doped ZnO Σ7 GB was described in Ref. 4. We analyzed coordination structure around Pr and electronic structure of the Pr-O bonds at the ZnO Σ7 GB for the present study.) Figure 4(k) shows the VCDP along Pr-O bonds at the Pr-doped ZnO Σ7 GB. There is also a similar tendency that VCDPs along Pr-O bonds at the ZnO Σ7 GB, when compared with those in Pr-doped ZnO crystal bulk, became closer to those of stable Pr_2O_3 crystals bulk. Also, there were five neighboring O around the Pr at the ZnO Σ7 GB as well. This indicates that the present findings are not specific to the ZnO Σ49 GB. At Pr-doped ZnO GBs, charge compensation may be required because Pr^{3+} substitute Zn^{2+} sites. We think that charge compensation can occur through the formation of acceptor-like native defects such as Zn vacancy.[4] The location and distribution of such defects may have some effects on the location of Pr. However, present results strongly suggest that location of Pr can be basically understood by considering atomic and electronic structure of Pr at the ZnO GB.

An important issue to be further investigated in future is occupancy of Pr along the atomic columns. The occupancy is directly related to how many Pr actually segregate per a unit area of the GB. The understanding will require atomic-scale three-dimensional observations (e.g., Ref. 30) of the GB. However, despite of the ambiguity of the occupancy, the present result clearly shows that Pr selectively segregates at the specific atomic columns of the GB. From the present finding, number of available Zn sites for Pr segregation at the GB can be understood. Since GB atomic arrangement varies with the GB orientation relationship and the GB plane, available sites for segregation should depend on the variation of the GB atomic arrangements. This may be one of the reasons why different GBs have different amounts of segregations, as was previously suggested in metals.[6]

IV. SUMMARY

We observed the atomic arrangement and location of Pr at a ZnO [0001] Σ49 GB by HAADF STEM. It was found that Pr segregated at three kinds of atomic columns of the ZnO Σ49 GB. Pr substituted at Zn sites in these atomic columns.

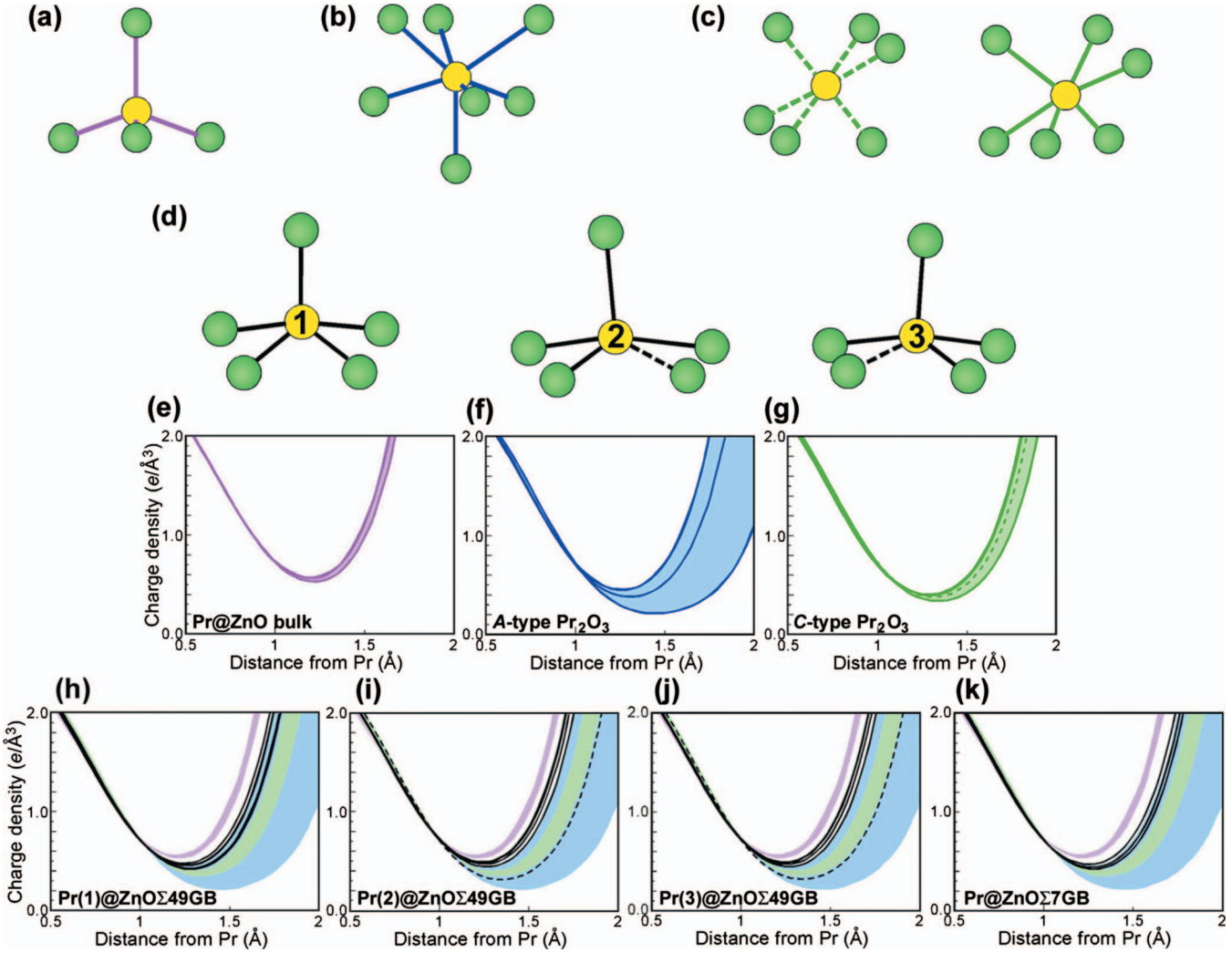

FIG. 4. (Color) (a)–(d) Schematics showing coordination structure around Pr in (a) Pr-doped ZnO, (b) *A*-type Pr_2O_3, and (c) *C*-type Pr_2O_3 crystals bulk, and at (d) Pr-doped ZnO Σ49 GB. Yellow and green circles show Pr and O, and lines between Pr and O indicate Pr-O bonds. Two different Pr are present for *C*-type Pr_2O_3 bulk in (c). Pr-O bonds of one Pr are shown by dotted lines (left panel), and those of the other are shown by solid lines (right panel). Three different Pr at the Pr-doped ZnO Σ49 GB in (d) are designated by "1," "2," and "3." For Pr(2) and Pr(3), one of Pr-O bonds is longer than the others, which is represented by the dotted line. (e)–(g) VCDP along the Pr-O bonds in (e) Pr-doped ZnO bulk, (f) *A*-type Pr_2O_3 bulk, and (g) *C*-type Pr_2O_3 bulk. Lines show VCDPs along respective Pr-O bonds, and hatches indicate regions of the VCDPs. Dotted lines in (g) correspond to the dotted lines in (c). (h), (i), and (j) show VCDP for Pr(1), Pr(2), and Pr(3) at the Pr-doped ZnO Σ49 GB. (k) VCDP for Pr at the Pr-doped Σ7 ZnO GB.[4] Black lines show the VCDPs for respective Pr-O bonds. Hatches in (e)–(g) are superimposed for comparison. Dotted lines in (i) and (j) correspond to the dotted lines in (d).

Framework structure of the Pr-doped ZnO Σ49 GB was similar to that of the undoped ZnO Σ49 GB, indicating that atomic arrangement of the ZnO Σ49 GB did not significantly change with the Pr doping. It was found that Zn-O interatomic distances of the three Zn sites were the longest. This accords with the concept of size misfit as has been suggested in previous papers.[6] There was a tendency for lengths and electronic structures of Pr-O bonds at the Pr-doped ZnO Σ49 GB, when compared with those in the Pr-doped ZnO crystal bulk, to be closer to those in *A*-type and *C*-type Pr_2O_3 crystals bulk. This indicates that Pr selectively segregates at these Zn sites at the ZnO Σ49 GB because the local atomic and electronic environments, when compared with those in ZnO crystal bulk, are closer in its thermodynamically stable form, Pr_2O_3.

ACKNOWLEDGMENTS

This work was supported in part by Japan Society for the Promotion of Science and the Grant-in-Aid for Scientific Research on Priority Areas "Nano Materials Science for Atomic-Scale Modification 474" from the Ministry of Education, Culture, Sports, and Technology (MEXT) of Japan.

[1] J. P. Buban, K. Matsunaga, J. Chen, N. Shibata, W. Y. Ching, T. Yamamoto, and Y. Ikuhara, Science **311**, 212 (2006).
[2] N. Shibata, S. J. Pennycook, T. R. Gosnell, G. S. Painter, W. A. Shelton, and P. F. Becher, Nature (London) **428**, 730 (2004).
[3] G. Duscher, M. F. Chisholm, U. Alber, and M. Rühle, Nature Mater. **3**, 621 (2004).
[4] Y. Sato, J. P. Buban, T. Mizoguchi, N. Shibata, M. Yodogawa, T. Yamamoto, and Y. Ikuhara, Phys. Rev. Lett. **97**, 106802 (2006).
[5] Y. Yan, M. F. Chisholm, G. Duscher, A. Maiti, S. J. Pennycook, and S. T. Pantelides, Phys. Rev. Lett. **81**, 3675 (1998).
[6] A. P. Sutton and R. W. Balluffi, *Interfaces in Crystalline Materials* (Oxford University Press, New York, 1995).
[7] D. R. Clarke, J. Am. Ceram. Soc. **82**, 485 (1999).
[8] D. G. Brandon, B. Ralph, S. Rangathan, and M. S. Wald, Acta Metall. **12**, 813 (1964).
[9] P. E. Blöchl, Phys. Rev. B **50**, 17953 (1994).
[10] G. Kresse and J. Furthmüller, Phys. Rev. B **54**, 11169 (1996).
[11] J. P. Perdew, K. Burke, and M. Ernzerhof, Phys. Rev. Lett. **77**, 3865 (1996).
[12] G. Adachi and N. Imanaka, Chem. Rev. (Washington, D.C.) **98**, 1479 (1998).
[13] S.-Y. Chun, N. Wakiya, H. Funakubo, K. Shinozaki, and N. Mizutani, J. Am. Ceram. Soc. **80**, 995 (1997).
[14] J.-L. Zhao, W. Zhang, X.-M. Li, J.-W. Feng, and X. Shi, J. Phys.: Condens. Matter **18**, 1495 (2006).
[15] F. Oba, A. Togo, I. Tanaka, J. Paier, and G. Kresse, Phys. Rev. B **77**, 245202 (2008).
[16] J. Albertsson, S. C. Abrahams, and Å. Kvick, Acta Crystallogr., Sect. B: Struct. Sci. **45**, 34 (1989).
[17] N. Hirosaki, S. Ogata, and C. Kocer, J. Alloys Compd. **351**, 31 (2003).
[18] O. Greis, R. Ziel, B. Breidenstein, A. Haase, and T. Petzel, J. Alloys Compd. **216**, 255 (1994).
[19] R. W. Wyckoff, *Crystal Structures*, 2nd ed. (Jon Wiley & Sons, New York, 1964), Vol. 2.
[20] J. D. Gale and A. L. Rohl, Mol. Simul. **29**, 291 (2003).
[21] Y. Sato, T. Mizoguchi, F. Oba, Y. Ikuhara, and T. Yamamoto, Phys. Rev. B **72**, 064109 (2005). The number of atoms in the supercell used in Ref. 21 was 448 atoms. In this study, supercell containing smaller number of atoms (224 atoms) was employed to use the first-principles calculations. GB atomic arrangement did not change significantly with the use of 224-atom supercell.
[22] H. J. Monkhorst and J. D. Pack, Phys. Rev. B **13**, 5188 (1976).
[23] Y. Sato, F. Oba, M. Yodogawa, T. Yamamoto, and Y. Ikuhara, J. Appl. Phys. **95**, 1258 (2004).
[24] S. J. Pennycook and D. E. Jesson, Phys. Rev. Lett. **64**, 938 (1990).
[25] S. J. Pennycook, in *Advances in Imaging and Electron Physics*, edited by P. G. Merli, G. Calestani, and M. Vittori-Antisari (Academic Press, London, 2002), Vol. 123, p. 173.
[26] Z. Hu, G. Kaindl, H. Ogasawara, A. Kotani, and I. Felner, Chem. Phys. Lett. **325**, 241 (2000).
[27] R. C. Karnatak, J.-M. Esteva, H. Dexpert, M. Gasgnier, P. E. Caro, and L. Albert, Phys. Rev. B **36**, 1745 (1987).
[28] R. D. Shannon, Acta Crystallogr., Sect. A: Cryst. Phys., Diffr., Thoer. Gen. Crystallogr. **A32**, 751 (1976).
[29] It is considered that Zn at **2** and **3** of the undoped ZnO GB has four nearest neighbor O. Thus, the longer Pr-O bonds were formed with replacing the Zn with Pr. Distance between the Zn and the O was ~2.70 Å, which was longer than length of Zn-O bonds in ZnO bulk by more than 34%. On the other hand, lengths of the longer Pr-O bonds (~2.50 or ~2.51 Å) for Pr(2) and Pr(3) was similar to those of Pr-O bonds in Pr_2O_3 bulks.
[30] K. van Benthem, A. R. Lupini, M. Kim, H.-S. Baik, S. Doh, J.-H. Lee, M. P. Oxley, S. D. Findlay, L. J. Allen, J. T. Luck, and S. J. Pennycook, Appl. Phys. Lett. **87**, 034104 (2005).